

Multi-omics Analysis Reveals Immune Features Associated with Immunotherapy Benefit in Patients with Squamous Cell Lung Cancer from Phase III Lung-MAP S1400I Trial



Edwin Roger Parra¹, Jieixin Zhang², Dzifa Yawa Duose¹, Edgar Gonzalez-Kozlova^{3,4,5,6}, Mary W. Redman⁷, Hong Chen⁸, Ganiraju C. Manyam², Gayatri Kumar¹, Jianhua Zhang⁹, Xingzhi Song⁹, Rossana Lazcano¹, Mario L. Marques-Piubelli¹, Caddie Laberiano-Fernandez¹, Frank Rojas¹, Baili Zhang¹, Len Taing¹⁰, Aashna Jhaveri¹⁰, Jacob Geisberg¹⁰, Jennifer Altreuter¹⁰, Franziska Michor¹⁰, James Provencher¹⁰, Joyce Yu¹⁰, Ethan Cerami¹⁰, Radim Moravec¹¹, Kasthuri Kannan¹, Rajyalakshmi Luthra¹², Gheath Alatrash¹³, Hsin-Hui Huang^{5,14}, Hui Xie⁵, Manishkumar Patel¹⁵, Kai Nie⁵, Jocelyn Harris⁵, Kimberly Argueta⁵, James Lindsay¹⁵, Roshni Biswas¹⁵, Stephen Van Nostrand^{10,15}, Seunghee Kim-Schulze^{3,4,5,6}, Jhanelle E. Gray¹⁶, Roy Herbst¹⁷, Ignacio I. Wistuba¹, Scott Gettinger¹⁶, Karen Kelly¹⁸, Lyudmila Bazhenova¹⁹, Sacha Gnjatic^{3,4,5,6}, J. Jack Lee²⁰, Jianjun Zhang^{8,9}, and Cara Haymaker¹

ABSTRACT

Purpose: Identifying molecular and immune features to guide immune checkpoint inhibitor (ICI)-based regimens remains an unmet clinical need.

Experimental Design: Tissue and longitudinal blood specimens from phase III trial S1400I in patients with metastatic lung squamous cell carcinoma (SqNSCLC) treated with nivolumab monotherapy (nivo) or nivolumab plus ipilimumab (nivo+ipi) were subjected to multi-omics analyses including multiplex immunofluorescence (mIF), nCounter PanCancer Immune Profiling Panel, whole-exome sequencing, and Olink.

Results: Higher immune scores from immune gene expression profiling or immune cell infiltration by mIF were associated with response to ICIs and improved survival, except regulatory T cells, which were associated with worse overall survival (OS) for patients receiving nivo+ipi. Immune cell density and closer proximity of CD8+GZB+ T cells to malignant cells were associated with

superior progression-free survival and OS. The cold immune landscape of NSCLC was associated with a higher level of chromosomal copy-number variation (CNV) burden. Patients with *LRP1B*-mutant tumors had a shorter survival than patients with *LRP1B*-wild-type tumors. Olink assays revealed soluble proteins such as LAMP3 increased in responders while IL6 and CXCL13 increased in nonresponders. Upregulation of serum CXCL13, MMP12, CSF-1, and IL8 were associated with worse survival before radiologic progression.

Conclusions: The frequency, distribution, and clustering of immune cells relative to malignant ones can impact ICI efficacy in patients with SqNSCLC. High CNV burden may contribute to the cold immune microenvironment. Soluble inflammation/immune-related proteins in the blood have the potential to monitor therapeutic benefit from ICI treatment in patients with SqNSCLC.

¹Departments of Translational Molecular Pathology, The University of Texas MD Anderson Cancer Center, Houston, Texas. ²Department of Bioinformatics and Computational Biology, The University of Texas MD Anderson Cancer Center, Houston, Texas. ³Department of Oncological Sciences, Mount Sinai, New York, New York. ⁴Tisch Cancer Institute, Mount Sinai, New York, New York. ⁵Precision Immunology Institute, Mount Sinai, New York, New York. ⁶Icahn School of Medicine at Mount Sinai, New York, New York. ⁷SWOG Statistical Center; Fred Hutchinson Cancer Research Center, Seattle, Washington. ⁸Department of Thoracic-Head and Neck Medical Oncology, The University of Texas MD Anderson Cancer Center, Houston, Texas. ⁹Department of Genomic Medicine, The University of Texas MD Anderson Cancer Center, Houston, Texas. ¹⁰CIMAC-CIDC Network, Pipeline Development and Portal integration, Dana-Farber Cancer Institute, Boston, Massachusetts. ¹¹Cancer Diagnosis Program, Division of Cancer Treatment and Diagnosis, NCI, Bethesda, Maryland. ¹²Department of Hematopathology, The University of Texas MD Anderson Cancer Center, Houston, Texas. ¹³Department of Stem Cell Transplantation, The University of Texas MD Anderson Cancer, Houston, Texas. ¹⁴Department of Population Health Science and Policy, Icahn School of Medicine at Mount Sinai, New York, New York. ¹⁵Department of Data Science,

Dana-Farber Cancer Institute, Boston, Massachusetts. ¹⁶Moffitt Cancer Center, Tampa, Florida. ¹⁷Yale Cancer Center, Yale School of Medicine, New Haven, Connecticut. ¹⁸International Association for the Study of Lung Cancer, Denver, Colorado. ¹⁹University of California San Diego Moores Cancer Center, La Jolla, California. ²⁰Department of Biostatistics, The University of Texas MD Anderson Cancer Center, Houston, Texas.

E.R. Parra, J. Zhang, D.Y. Duose, and E. Gonzalez-Kozlova contributed as co-first authors to this article.

Corresponding Authors: Cara Haymaker, The University of Texas MD Anderson Cancer Center, 7435 Fannin St, Houston, TX 77054. E-mail: chaymaker@mdanderson.org; and Jianjun Zhang, jzhang20@mdanderson.org

Clin Cancer Res 2024;XX:XX-XX

doi: 10.1158/1078-0432.CCR-23-0251

This open access article is distributed under the Creative Commons Attribution-NonCommercial-NoDerivatives 4.0 International (CC BY-NC-ND 4.0) license.

©2024 The Authors; Published by the American Association for Cancer Research

Translational Relevance

Identifying molecular and immune features to guide immune checkpoint inhibitor (ICI) regimens remains an unmet clinical need. We performed multi-omics analysis of biospecimens from a phase III trial LUNG-MAP S1400I that compared ipilimumab combined with nivolumab versus nivolumab monotherapy in patients with metastatic lung squamous cell carcinoma. An overall cold tumor immune microenvironment correlated with high chromosomal copy-number variant burden and was associated with inferior benefit from ICIs. In addition to the immune cell density, the proximity and local neighborhood clustering of a subset of immune cells to tumor cells also impacted the benefit from ICI therapy. Interestingly, patient survival was decreased with *LRP1B*-mutant tumors, but not with *LRP1B*-wild type tumors. Many soluble proteins related to inflammation or T-cell and dendritic cell activation correlated with clinical outcome from ICI therapy. Together, these immune features highlight the potential of biomarker-based strategies to select patients for ICI-based regimens and dynamically monitor their response.

its reliability as a predictive biomarker (16, 17). Although tumor mutational burden (TMB) has been approved as a predictive marker for anti-PD-1/PD-L1 treatment for melanoma and NSCLC, and several other cancer types (18), one study found no correlation between TMB or PD-L1 with anti-PD-1 plus anti-CTLA-4 therapy in patients with NSCLC (19). Furthermore, the predictive value of PD-L1 and TMB becomes less clear when chemotherapy is added. These findings underscore the complexity of molecular determinants of the tumor immune microenvironment and response to ICIs.

In this study, we sought to elucidate the immune and molecular mechanisms that affect benefit from ICIs in patients with advanced SqNSCLC. Toward this end, we integrated immune and multi-omics profiling platforms supported by Cancer Immune Monitoring and Analysis Centers (CIMAC) in the current study. Specifically, we performed multiplex immunofluorescence (mIF), gene expression profiling (nCounter PanCancer Immune Profiling Panel), whole-exome sequencing (WES), and Olink proteomics on tissue and blood specimens from the S1400I trial to identify molecular or immune factors associated with better prognoses in patients treated with anti-PD-1 monotherapy versus anti-PD-1/CTLA-4 dual combination.

Introduction

Immune checkpoint inhibitors (ICI) targeting programmed cell death protein 1 (PD-1, e.g., nivolumab, pembrolizumab, cemiplimab) or its ligand PD-L1 (e.g., atezolizumab) have become pillars of treatment in both frontline and salvage settings for patients with advanced non–small cell lung cancer (NSCLC; refs. 1–4). In addition, recent efforts have led to multiple approved frontline regimens incorporating chemotherapy and other ICIs with anti-PD-1/PD-L1 antibodies (5–8). However, in the salvage setting, anti-PD-1/PD-L1 monotherapy remains the treatment of choice for ICI-naïve advanced-stage NSCLC (9, 10).

Ipilimumab is an ICI targeting CTL-associated protein 4 (CTLA-4). Its dual inhibition with PD-1/PD-L1 may have synergistic effects on the anticancer immune response, given the complementary functions of these two pathways. The combination of nivolumab with ipilimumab (nivo+ipi) was demonstrated to have superior efficacy than nivolumab alone in patients with advanced melanoma (11, 12). For patients with metastatic NSCLC, ipilimumab plus nivolumab has been approved by the FDA in the frontline setting with or without concurrent chemotherapy (7, 8, 13, 14). In the salvage setting, a recent phase III study, S1400I, evaluated the efficacy of nivo+ipi versus nivolumab monotherapy (nivo) in patients without previous ICI treatment for squamous NSCLC (SqNSCLC; ref. 15). The study did not show that ipilimumab plus nivolumab improved clinical outcomes. However, progression-free survival (PFS) and overall survival (OS) curves separated during later follow-up, suggesting that a subset of patients may benefit from combination treatment with ipilimumab and nivolumab.

Understanding the mechanisms underlying response and resistance to ICIs and establishing predictive molecular and immune features to identify patients who will benefit the most from ICI therapy remain unmet clinical needs. High PD-L1 expression is associated with improved outcomes in patients receiving ICI monotherapy (1, 8). However, the geographical heterogeneity of PD-L1 expression between primary tumors and metastatic sites and even between different regions within the same tumors—as well as the potential dynamic changes in PD-L1 expression over time—have raised questions about

Material and Methods

Study population and human tissue samples

Lung-MAP (S1400I, NCT02785952) was a multicenter, open-label, phase III randomized clinical trial. The substudy Lung-MAP-I (S1400I) was conducted from December 18, 2015, to April 23, 2018, through the National Clinical Trials Network and led by the SWOG Cancer Research Network. The study was conducted in accordance with the Declaration of Helsinki and the Lung-MAP design has been described previously (15). Briefly, the trial compared nivo+ipi with nivo in patients with chemotherapy-pretreated, immunotherapy-naïve, advanced sqNSCLC. Two hundred fifty-two patients were randomly assigned to receive nivo+ipi ($n = 125$) or nivo ($n = 127$). The clinical efficacy endpoints were OS, PFS, duration of response, and best objective response by RECIST 1.1. Each site required approval by the U.S. NCI central Institutional Review Board or approval by their local Institutional Review Board. Written, informed consent was required for all patients prior to registration.

Available tumor tissue samples and blood samples ($N = 160$, Supplementary Fig. S1) submitted for Lung-MAP screening were provided by the SWOG tissue bank. The clinical information for correlative studies in collaboration with the CIMAC–Cancer Immunologic Data Commons (CIDC) Network is shown in Supplementary Table S1 across the different assays.

mIF staining and analysis

mIF staining was performed in 82 screening tumor tissue samples (nivo+ipi = 38, and nivo = 42; Supplementary Table S1). Unstaining slides from formalin-fixed, paraffin-embedded (FFPE) tissue were received from the SWOG bank and stained using methods previously described and validated (20). Briefly, 4-μm-thick FFPE tumor sections were stained using an automated staining system (Leica Microsystems) and two mIF panels with the following antibodies: Panel 1, cytokeratin (CK), CD3, CD8, PD-1/PD-L1, and CD68 and Panel 2, CK, CD3, CD8, CD45RO, granzyme B (GZB), and FOXP3. Antibody clones, dilutions, and RRIDs are included in Supplementary Table S2 and have been described previously (20). All the markers were stained in sequence using their respective fluorophore contained in the Opal 7-Color Automation IHC Kit (catalog no. NEL821001KT; Akoya Biosciences). The slides were scanned using the Vectra/Polaris 3.0.3 (Akoya

148	Biosciences) at low magnification, $10 \times$ ($1.0 \mu\text{m}/\text{pixel}$) through the full	206
149	emission spectrum and positive tonsil controls from the run staining to	207
150	calibrate the spectral image scanner protocol (21). A pathologist	208
151	selected representative areas inside the tumor using regions of interest	209
152	for scanning in high magnification by the Phenochart Software image	210
153	viewer 1.0.12 ($931 \times 698 \mu\text{m}$ size at resolution $20 \times = 0.5 \mu\text{m}/\text{pixel}$) to	211
154	capture various elements of tissue heterogeneity. Marker coexpression	212
155	was employed to identify malignant cells (CK+), malignant cells	213
156	expressing PD-L1 (CK+PD-L1+), and the cellular subsets of	214
157	tumor-associated immune cells (TAIC) listed in Supplementary	215
158	Table S3. Densities of each cell phenotype were quantified as the	216
159	number of cells/ mm^2 in the tumor compartment characterized by	217
160	group or nests of malignant cells, in the stroma compartment char-	218
161	acterized by the fibrous tissue present between the tumor nets, and in	219
162	both compartments described as a total. PD-L1+ malignant cells were	220
163	also expressed in percentages. The data were consolidated using R	221
164	studio 3.5.3 (Phenopter 0.2.2 packet; Akoya Biosciences).	
165	Spatial point pattern distribution analysis	222
166	Using the point pattern distribution of the cell phenotypes relative	223
167	to malignant cells, we measured the distance from malignant cells	224
168	(CK+) to TAICs included in each mIF panel using R studio 3.5.3	225
169	(Phenopter 0.2.2 packet). We applied the median nearest neighbor	226
170	function from malignant cells (CK+) to different cell phenotypes to	227
171	determine where these TAICs were located; specifically, whether the	228
172	TAICs were close to (i.e., equal to or less than the median distance) or	229
173	far from (i.e., more than the median distance) the malignant cells	230
174	(CK+) and associated with clinical outcomes.	231
175	Spatial organization of cells by type	232
176	Cells were subset by phenotype using the markers in the mIF panels	233
177	and examined as the following: Tumor/PD-L1+ (CK+PD-L1+), Tumor	234
178	(CK+), Other-Tcells (CD3+), Other-Tcells/PD-1+ (CD3+PD-1+),	235
179	Macrophages(CD68+), Macrophages/PD-L1+(CD68+PD-L1+),	236
180	CTLs(CD3+CD8+), CTLs/PD-1+(CD3+CD8+PD-1+), CTLs/GB+	237
181	(CD3+CD8+GB+), and Tregs (CD3+CD8–Foxp3+). The above	238
182	phenotypes were used to visualize the spatial organization of cells by	239
183	type. This analysis was carried out in R version 4.2.0 (R studio 2022.07.2).	240
184	Spatial neighborhood	241
185	Using the marked planar point pattern representations of each mIF	242
186	image, we calculated the spatially varying probabilities for each of the	243
187	phenotypes (described above). We used the spatstat toolbox (22)	244
188	which provides the relrisk function to identify areas of segregation	245
189	for a multitype (markers >2) marked point pattern. This function	246
190	estimates for each phenotype, the spatially varying probability or the	247
191	ratios of the probabilities, using kernel smoothing. The output of this	248
192	function was used to plot the contour of the spatially segregated	249
193	neighborhoods for each phenotype.	250
194	Identifying cell clusters in the local neighborhood	251
195	We identified cell clusters in each image using Euclidean distance	252
196	and a hierarchical clustering method. A minimum cluster size of 10	253
197	cells and distance $\leq 20 \mu\text{m}$ was the requirement for clustering. The	254
198	distance-based hierarchical clustering yielded the neighborhood	255
199	information in a matrix. The cells that did not form clusters were	256
200	labeled "Free_cell". The relative percentages of cells in each phe-	257
201	notype within a cluster were used to generate the heat map. We used	258
202	the SPIAT library (SPIAT version 1.0.4) to identify cell clusters and	259
203	made additions to the SPIAT functions as required for our analysis	260
204	using R version 4.2.0.	261
	NanoString gene expression profiling	262
	DNA and RNA were coextracted from FFPE specimens received	263
	from the SWOG bank (Supplementary Table S1) and subjected to WES	
	and gene expression. The RNA from a total of 38 FFPE samples (nivo =	
	23 and nivo+ipi = 15) passed the quality control (QC) and was run on	
	the nCounter platform using the PanCancer Immune Profiling Panel	
	(730 immune-related and 40 housekeeping genes) per the manufac-	
	turer's instructions. Briefly, samples were hybridized overnight at 65°C	
	to probes, excess probes were washed using the automated prep station	
	and then imaged on the digital analyzer. All runs included a Human	
	Reference RNA control for batch correction. Data were processed and	
	normalized with NanoString's nSolver analysis software (23). All	
	samples passed the post-run QC metrics, and no batch effects were	
	evident in the runs. In addition, gene expression profiles were decon-	
	voluted by TIMER and nSolver advanced analysis tools to infer	
	immune cells correlated to clinical outcomes.	
	WES data analysis	222
	WES analysis was conducted using the CIDC WES pipeline on	223
	tumor DNA from 50 tumors (nivo = 28 and nivo+ipi = 22, Supple-	224
	mentary Table S1) that passed the QC. DNA from paired peripheral	225
	blood mononuclear samples was used as germ line control. WES	226
	implements Gene Analysis Toolkit (24) best practices and identifies	227
	somatic variants using Sentieon TNScope and Haplotype algorithms	228
	(25), respectively. Somatic variants are annotated using the	229
	Variant Effect Predictor software (26). The pipeline uses an ensemble	230
	of three callers, CNVkit (27), Sequenza (28), and Facets (29), to	231
	characterize tumor copy-number variation (CNV), and the CNV	232
	segments called by at least two callers were used to generate a high-	233
	confident consensus set. Sequenza and FACETS were used to estimate	234
	tumor purity and also PyClone-VI was utilized to infer clonal status of	235
	mutations (30). PyClone v 0.13.1 (31) was used to perform mutation	236
	clonality analysis. It is a Bayesian clustering method that enables	237
	mutations to be grouped into putative clonal clusters by integrating	238
	copy number, tumor purity (obtained from Sequenza), and variant	239
	allele frequency data.	240
	Olink serum soluble analyte assay	241
	We performed circulating serum analyte measurements using	242
	proximity extension assay (Olink) in 561 serum samples collected	243
	longitudinally from 160 patients (Supplementary Table S1). A series of	244
	92 proteins, such as cytokines and soluble immune checkpoints	245
	included in the "immuno-oncology" panel, was measured as described	246
	previously (32). Protein levels were normalized using internal positive	247
	and negative controls and quantified as \log_2 protein expressions	248
	(NPX), which were subsequently used as input for downstream	249
	analysis.	250
	Correlative analysis and statistical methods	251
	To evaluate whether the baseline biomarkers are prognostically	252
	associated with survival, we dichotomized biomarker data by the	253
	median and performed univariate survival analysis with the log-	254
	rank test. OS and PFS were evaluated. The Cox proportional hazards	255
	regression model was used for multivariate survival analysis (R	256
	package Survival, https://CRAN.R-project.org/package=survival ; ref. 33). We included TMB (≥ 10 or < 10 mutations per Mb), PD-L1	257
	(≥ 5 or $< 5\%$), and other statistically significant biomarkers identified	258
	from univariate analysis in Cox models. Thresholds for TMB and PD-	259
	L1 were determined from previous clinical studies (18). To assess	260
	whether continuous biomarker data are associated with response and	261
	other clinical variables, we used nonparametric tests: Spearman rank	262
		263

correlation for continuous clinical variables, Mann–Whitney U test for categorical clinical variables with two groups, and Kruskal–Wallis test for categorical variables with more than two groups. In parallel, we also dichotomized biomarker data and used the χ^2 test for a robust assessment with responders. The Benjamini–Hochberg method (34) was used for multiple testing adjustment of <i>P</i> values. The analysis was performed on all samples and on samples in two treatment arms separately.	mIF markers from different compartments along with Olink proteins. The minimum number of observations in a node for a split was set to be 15; 10-fold cross-validation was carried out and results used for tree-pruning. For RF, we used 81 samples with both Olink and mIF data. Bootstrap the data to create bootstrap samples; grow a survival tree for each bootstrap sample with split criteria based on the log-rank statistics; continue the recursive partition; and calculate importance of each predictor by averaging over the forest.	328 329 330 331 332 333 334 335
To explore the association of each baseline protein level with clinical outcomes from the Olink data, we used logistic regression models for best objective response and Cox proportional hazards models for PFS and OS (R package Survival, https://CRAN.R-project.org/package=survival , RRID: SCR_021137; ref. 33). In separate regression models, univariate analyses included only the protein expression values, while the multiple variable analyses adjusted for additional covariates (i.e., treatment, age, sex, race, smoking). Then, to investigate the longitudinal changes in serum protein associated with treatment, we used mixed linear models (R package Dream and lme4; refs. 35, 36) and the timepoints baseline, cycle 2 week 3, cycle 4 week 7, and cycle 5 week 9 to quantify the effect of these variables and additional relevant clinical parameters. These were analyzed with the treatment arms nivo+ipi and nivo. In our models, each protein NPX was considered an independent variable. In contrast, phase, timepoints, and treatments were considered dependent variables and other covariates as random effects. This approach allowed us to quantify the variance across proteins and approximate degrees of freedom of the hypothesis test for each protein, thereby minimizing false-positive results. We used F-tests for multiple coefficient comparisons and moderate <i>t</i> tests for single coefficient comparisons.	In conjunction with the clinical study principal investigator/chair, the NCI-sponsored network and CIDE, we will make available de-identified data publicly available by request under the dbGaP PHS accession number: phs003412.v1.p1. Questions and requests for additional data can be directed to the corresponding author.	336 337 338 339 340 341
Results		342
Clinical characteristics		343
There were 31 responders (19.4%), including complete responses, partial responses, and unconfirmed partial/complete response; 63 patients with stable disease (39.4%); and 61 patients (38.1%) with progressive disease (i.e., increasing disease and symptomatic deterioration). Overall, 31 patients (19.4%) were alive at the end of the study, and the median OS was 10.02 months (range: 0.3–40.3). One hundred and forty-eight patients (92.5%) had disease progression, with a median PFS of 3.4 months (range: 0.3–36.6; Supplementary Table S1).	344 345 346 347 348 349 350 351	
An active immune infiltration is associated with benefit from ICI treatment		352 353
We first analyzed the mIF and gene expression profiling data from baseline tissue samples taken before ICI treatment to identify immune features associated with clinical benefit. mIF data revealed higher densities of various immune cells in the stroma compartment compared with the tumor compartment across the whole cohort (nivo+ipi and nivo arms), with no significant differences between the nivo+ipi and nivo arms (Supplementary Table S4). The overall immune cell densities were higher in the responders across both arms, although the difference did not reach statistical significance. In the whole cohort, higher median densities of PD-1+ cytotoxic T cells (CTL; CD3+CD8+PD-1+) in the stroma (>4.1 cells/mm 2 , <i>P</i> = 0.042), presence of GZB+ CTLs in the tumor compartment (>0 cells/mm 2 , <i>P</i> = 0.011), and higher median densities of memory T cells (CD3+CD45RO+; >23.4 cells/mm 2 , <i>P</i> = 0.041) and PD-1+ T cells (CD3+PD-1+; >16.0 cells/mm 2 , <i>P</i> = 0.023) in the total compartment (tumor plus stroma) were associated with longer PFS (Supplementary Table S5). Similarly, transcriptomic analysis demonstrated that patients having tumors with a higher expression of genes associated with myeloid infiltration, immune recruitment, and inflammation had superior clinical outcomes in the whole cohort (Table 1; Supplementary Table S6). The associations between higher expression of CD163, BLNK, IRF1, FCGR2A with better OS (<i>P</i> < 0.05) and higher expression of MAPK11 with worse OS remained significant in subsequent multivariate analyses after adjustments for known predictive biomarkers, including TMB and PD-L1.	354 355 356 357 358 359 360 361 362 363 364 365 366 367 368 369 370 371 372 373 374 375 376 377 378	
For integrative analysis, we applied recursive partitioning tree analysis (RPART, rpart library in R, https://cran.r-project.org/web/packages/rpart/vignettes/longintro.pdf) and random forest (refs. 41, 42; RF, randomForest and randomForestSRC libraries in R) on Olink (<i>N</i> = 159) and mIF (<i>N</i> = 82) data. We fitted RPART tree using responder status as the dependent variable, 92 baseline level Olink proteins and 17 mIF markers as predictors. We also created decision tree survival prediction model. Separate RPART trees were fitted for	In the nivo arm, higher densities of memory T cells (CD3+CD45RO+) in the total compartment (median >24.6 cells/mm 2 , <i>P</i> = 0.028) and memory/regulatory T cells (Treg; CD3+CD8-CD45RO+FOXP3+) in the total compartment (median >4.6 cells/mm 2 , <i>P</i> < 0.001) and the stroma compartment (median >12.0 cells/mm 2 , <i>P</i> = 0.049) were associated with longer PFS (Table 2; Fig. 1A and B).	379 380 381 382 383 384

Q6

Table 1. Associations of genes with outcomes by arm using NanoString.

Arm	Gene	Outcome	HR	CI	P
nivo	FADD	OS	3.63	1.32-9.93	0.002
	CLEC4C	OS	3.06	1.16-8.09	0.009
	DNAJC14	OS	2.96	1.13-7.79	0.010
	CREB5	PFS	4.04	1.41-11.56	<0.001
	FADD	PFS	2.79	1.08-7.19	0.007
	IL19	PFS	2.65	1.04-6.75	0.009
	PIN1	PFS	0.36	0.15-0.90	0.005
nivo+ipi	CCL22	OS	4.26	1.16-15.66	0.006
	CD163	OS	0.21	0.06-0.71	0.007
	CXCL10	OS	0.22	0.06-0.74	0.009
	CXCL11	OS	0.22	0.06-0.74	0.009
	IFI27	OS	0.22	0.07-0.76	0.010
	ITGB3	OS	0.17	0.05-0.62	0.002
	MAPK11	OS	4.48	1.20-16.68	0.004
	MAPK8	OS	0.19	0.06-0.67	0.004
	CIR	PFS	0.22	0.07-0.75	0.010
	CIS	PFS	0.21	0.06-0.71	0.007
	CD163	PFS	0.18	0.05-0.64	0.002
	ETS1	PFS	0.19	0.06-0.67	0.004
	FCGR2A	PFS	0.20	0.06-0.69	0.004
	IL15RA	PFS	0.22	0.07-0.75	0.010
	IL32	PFS	0.19	0.06-0.67	0.004
	ITGB3	PFS	0.17	0.05-0.60	0.001
	MAPK8	PFS	0.20	0.06-0.71	0.006
	PRKCD	PFS	0.19	0.05-0.66	0.004
	STAT2	PFS	0.22	0.06-0.74	0.009

Abbreviations: nivo, nivolumab; nivo+ipi, nivolumab plus ipilimumab; OS, overall survival; PFS, progression-free survival.

Higher densities of memory/Tregs (CD3+CD8-CD45RO+FOXP3+) in the total compartment (median > 4.6 cells/mm², *P* = 0.026) were associated with better OS (Table 2; Fig. 1C). In the nivo+ipi arm, higher densities of PD-1+ T cells (CD3+PD-1+) in the total compartment (median > 16.0 cells/mm², *P* = 0.0347) and the presence of GZM+ CTLs (CD3+CD8+GZB+) in the tumor compartment (>0 cells/mm², *P* = 0.0154) were associated with longer PFS (Table 2; Fig. 1D and E). Conversely, higher densities of Tregs (CD3+CD8-FOXP3+) in the total compartment (median > 12.4 cells/mm², *P* = 0.0418) were associated with worse OS (Table 2; Fig. 1F). In the nivo+ipi arm, deconvolution of transcriptomic profiling data by TIMER and nSolver demonstrated significantly higher total immune cells (CD45+), a higher exhausted CD8+ T-cell score, and a higher neutrophil score in responders versus nonresponders (*P* < 0.05, Fig. 1G-I), further supporting that overall higher immune infiltration is associated with superior clinical benefit from ICI treatment.

High infiltration of CTLs is associated with exceptional response to ICIs

Next, we specifically investigated exceptional responders, defined as patients who had no progression for at least 18 months and were still alive by 24 months, versus early progressors, who survived more than 1 month but had progressive disease and died within 6 months after initiating ICI treatment. By these definitions, there were 11 exceptional responders and 44 early progressors across the total trial cohort (Fig. 2A). There were more exceptional responders in the nivo+ipi arm than in the nivo arm (7 of 73 vs. 4 of 87, *P* = 0.35). Among these patients, 8 exceptional responders and 21 early progressors had tissues available for mIF, and 6 exceptional responders and 8 early progressors had tissues available for gene expression analysis.

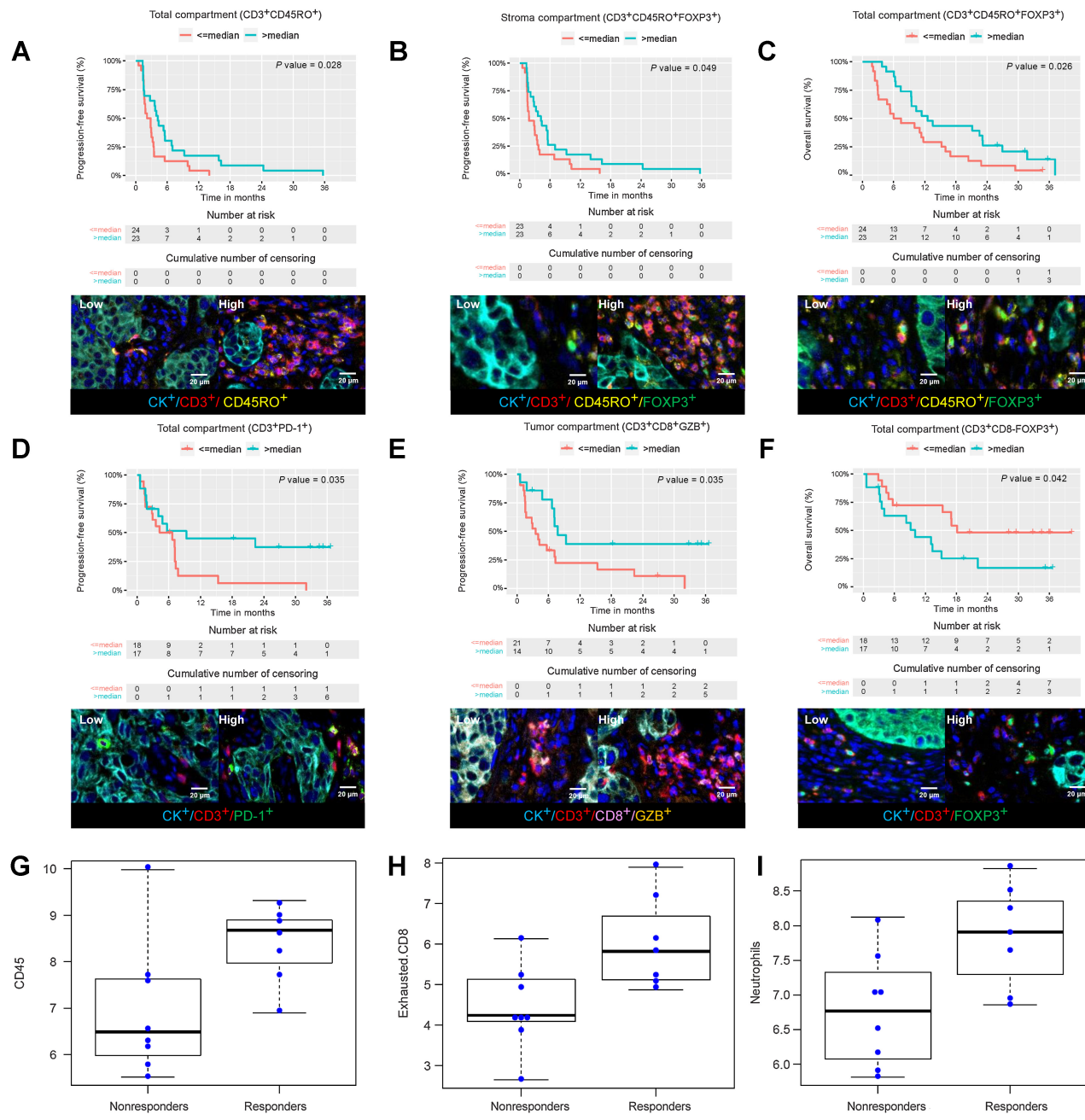
By mIF, we observed higher densities of CTLs (CD3+CD8+) and memory CTLs (CD3+CD8+CD45RO+) in the total compartment in exceptional responders than in early progressors (CTLs: median, 152.1 vs. 27.3 cells/mm²; *P* = 0.032; memory CTLs: median, 31.2 vs. 2.1 cells/mm²; *P* = 0.040; Supplementary Table S7). Representative images from an exceptional responder are shown in Fig. 2B and C. Moreover, in the tumor compartment, we observed higher densities of GZB+ CTLs (CD3+CD8+GZB+) in the exceptional responders than the early progressors (median, 3.6 vs. 0 cells/mm², *P* = 0.027; Fig. 2D). Representative images from an early progressor showing a lower density of immune infiltration are shown in Fig. 2E and F.

Furthermore, distinctive spatial neighborhoods and cell organization in tumor microenvironment (TME) were observed in exceptional responders (*n* = 6) relative to early progressors (*n* = 6; Fig. 2G-J; Supplementary Figs. S2 and S3). Shown in Fig. 2G; Supplementary Figs. 2A and 3A is the distribution of different cell subsets relative to each other, with higher immune infiltration and higher CTL densities in the TME of exceptional responders versus early progressors. We then used spatially varying probabilities of different cell phenotypes to determine the segregation among immune subsets and malignant cells, and a contour plot to represent the neighborhoods within the TMEs. These analyses revealed a higher spatial segregation of immune cell subsets relative to malignant cells in the early progressors as compared with the exceptional responders (Fig. 2H; Supplementary Figs. S2B and S3B) in line with above observation that higher densities of CTLs in the tumor region positively associated with survival. Through distance-based hierarchical clustering, we identified local cell clusters within the TME and observed distinct compositions in exceptional responders versus early progressors. The clusters (cells ≥ 10 within interacting distance 20 μm) in exceptional responders often consisted of CTLs and other T-cell populations in the proximity to tumor cells (Fig. 2I and J; Supplementary Figs. S2C, S2D, S3C, and S3D). Finally, infiltration of neutrophils inferred from gene expression profiling data was significantly higher in exceptional responders than early progressors (*P* = 0.029; Supplementary Fig. S4).

Table 2. Associations between cell phenotypes by compartment and by treatment arm.

Arm	Compartment	Cell phenotype	Outcome	HR	CI	P
nivo+ipi	Tumor	CD3+CD8+GZB+	PFS	0.38	0.18-0.81	0.015
		CD3+CD8-FOXP3+	OS	2.33	0.99-5.51	0.042
	CD3+PD-1+	PFS	0.45	0.21-0.97	0.035	
nivo	Stroma	CD3+CD45RO+FOXP3+	PFS	0.58	0.32-1.05	0.049
		CD3+CD45RO+	PFS	0.55	0.31-1.00	0.028
		CD3+CD45RO+FOXP3+	OS	0.52	0.28-0.96	0.026
	Total	CD3+CD45RO+FOXP3+	PFS	0.42	0.23-0.78	<0.001

Abbreviations: nivo, nivolumab; nivo+ipi, nivolumab plus ipilimumab; GZB, granzyme B; Total, tumor plus stroma; PFS, progression-free survival.

**Figure 1.**

Kaplan-Meier survival curves of cellular densities and immune signatures. In the nivo arm, Kaplan-Meier survival curves show high cellular densities (>the median value used as cutoff) of memory T cells ($CD3^+CD45RO^+$; **A**) in the total compartment and $CD45RO^+$ Tregs ($CD3^+CD45RO^+FOXP3^+$; **B**) in the stroma compartment were associated with better PFS. **C**, $CD45RO^+$ Tregs ($CD3^+CD45RO^+FOXP3^+$) in the total compartment were associated with better OS. Representative multispectral images show low and high cell phenotype densities for **A-C**. In the nivo+ipi arm, the Kaplan-Meier survival curves show that high cellular densities of PD-1+ T cells ($CD3^+PD-1^+$; **D**) in the total compartment and GZB+ CTLs ($CD3^+CD8^+GZB^+$; **E**) in the total compartment were associated with better PFS. Conversely, **(F)** Tregs ($CD3^+CD8-FOXP3^+$) in the total compartment were associated with poor OS. Representative multispectral images show low and high cell phenotype densities for **D-F**. Cell scoring derived from gene expression profiling using nSolver shows higher scores for $CD45^+$ immune cells (**G**), $CD8^+$ T cells (**H**), and neutrophils (**I**) in responders compared with nonresponders in the nivo+ipi arm.

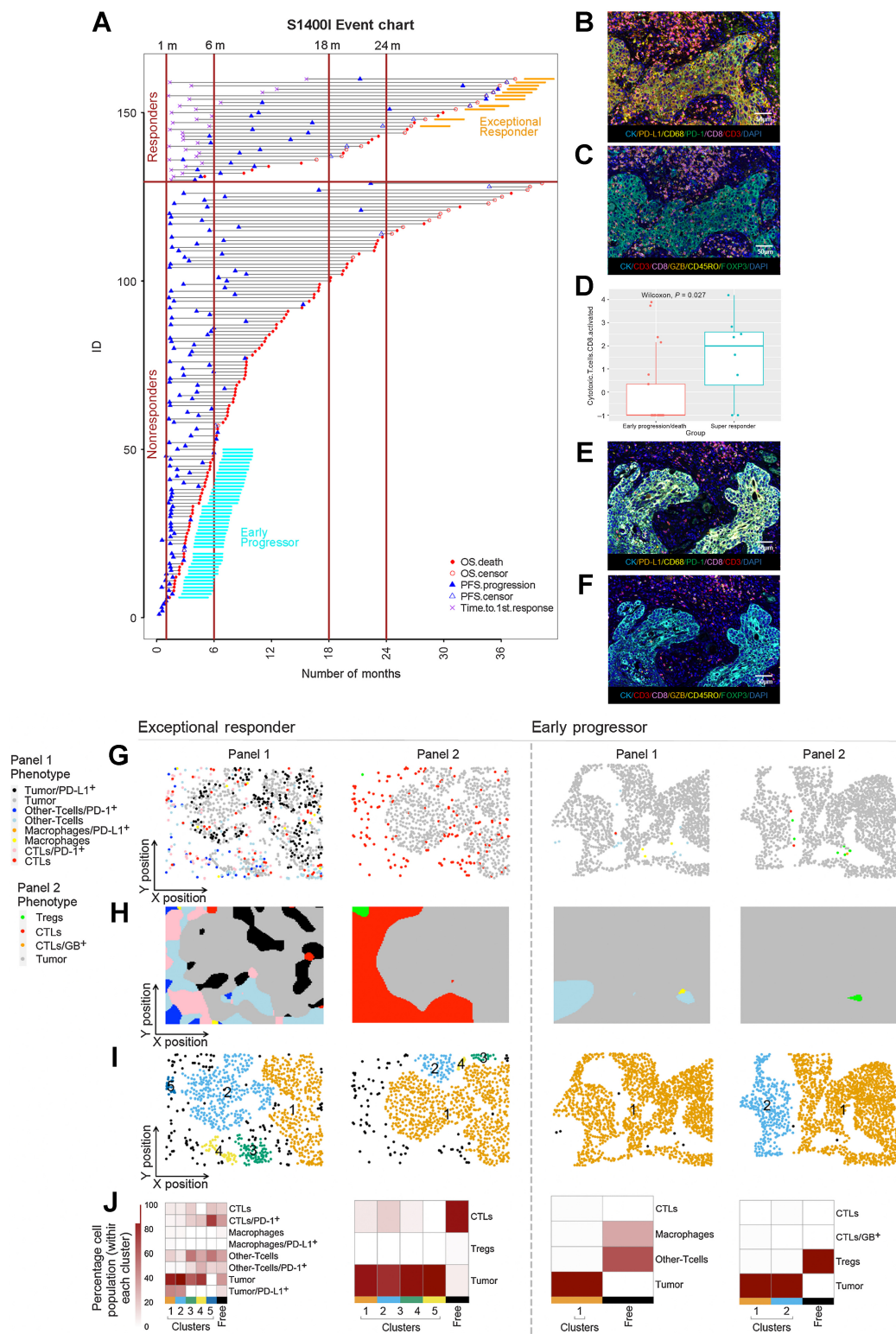
Q7

Close proximity of T cells and malignant cells is associated with benefit from ICIs

Given the recognized importance of distance between different cells and the clustering of CTLs and tumor cells observed in exceptional

responders, we expanded our analysis to understand the spatial relationship between the cell types associated with clinical outcome described above with other cells within the TME (43, 44). In the whole cohort, shorter distances from malignant cells (CK+) as well as

454
455
456
457459
460
461
462

**Figure 2.**

Immune infiltration in exceptional responders and early progression across the arms. **A**, The upper level of the event chart shows the exceptional responders, and the lower level shows the early progression/death group. The solid red circles represent deaths in the OS analysis, the open red circles indicate OS-censored patients, the solid blue triangles indicate progression in the PFS analysis, the open blue open triangles indicate PFS-censored patients, and the violet X indicates the time to the first response. (Continued on the following page.)

465 PD-L1+ malignant cells (CK+PD-L1+) to CTLs (CD3+CD8+; median,
 466 139 and 148 μ m) were associated with better PFS ($P = 0.045$ and
 467 $P = 0.027$, respectively); and shorter distances from malignant cells
 468 (CK+) to GZB+ CTLs (CD3+CD8+GZB+) were associated with
 469 significantly longer PFS ($P = 0.035$) and a trend toward longer OS
 470 ($P = 0.054$; Fig. 3A–E). In the nivo+ipi arm, shorter distances of CTLs
 471 (CD3+CD8+) as well as GZB+ CTLs (CD3+CD8+GZB+) from
 472 malignant cells (CK+; $P = 0.045$ and, $P = 0.026$, respectively) and
 473 shorter distances between CTLs (CD3+CD8+) from PD-L1+ malig-
 474 nant cells (CK+PD-L1+; $P = 0.033$) were associated with longer
 475 PFS (Fig. 3F–H). In addition, shorter distances of GZB+ CTLs
 476 (CD3+CD8+GZB+; median, 245 μ m) from malignant cells (CK+)
 477 were associated with longer OS ($P = 0.045$; Fig. 3I). Taken together,
 478 these results suggest that the immune cells' density and spatial distri-
 479 bution may impact response to ICI therapy.

High CNV burden is associated with cold immune infiltration

We next performed WES ($n = 50$) with the intent of identifying the genomic basis underlying the immune features associated with benefit from nivo+ipi versus nivo in these metastatic squamous cell carcinomas. A total of 30,081 nonsilent mutations were detected with transversions, particularly C>A, as the predominant substitutes, which was expected because most patients were smokers (Supplementary Fig. S5A). The commonly mutated cancer genes included *TP53*, *LRP1B*, *CDKN2A*, *ARID1A*, and *PIK3CA* (Supplementary Fig. S5B). High CNV burden was associated with a colder tumor immune microenvironment, as evidenced by lower infiltration levels of overall CD3⁺ T cells from mIF and lower levels of various immune signatures derived from gene expression profiling (Supplementary Fig. S6A and S6B). Importantly, CNV burden was not associated with estimated tumor purity, suggesting the correlation between high CNV burden and cold tumor immune microenvironment was not due to relative high tumor cell density leading to dilution of immune cells. Taken together, these results indicate that chromosomal instability may be an underlying genomic feature associated with immune evasion in metastatic SqNSCLC. Among the commonly mutated cancer genes, mutations in *LRP1B*, a recently recognized potential regulator of the inflammatory response, was associated with less infiltration of GZB+ CTLs (CD3+CD8+GZB+; Supplementary Fig. S7A; refs. 45, 46). Interestingly, *LRP1B* mutations were enriched in nonresponders but not in responders (18/19 vs. 2/11, $P = 0.049$). Furthermore, patients with *LRP1B* mutations had significantly ($P = 0.008$) shorter PFS (Supplementary Fig. S7B) and numerically shorter OS in the overall cohort (Supplementary Fig. S7C). *LRP1B*-mutant tumors were not associated with short PFS in the nivo+ipi arm (Supplementary Fig. S7D) but were in the nivo arm ($P = 0.033$; Supplementary Fig. S7E).

Dynamic changes in peripheral blood cytokines are associated with benefit from ICIs

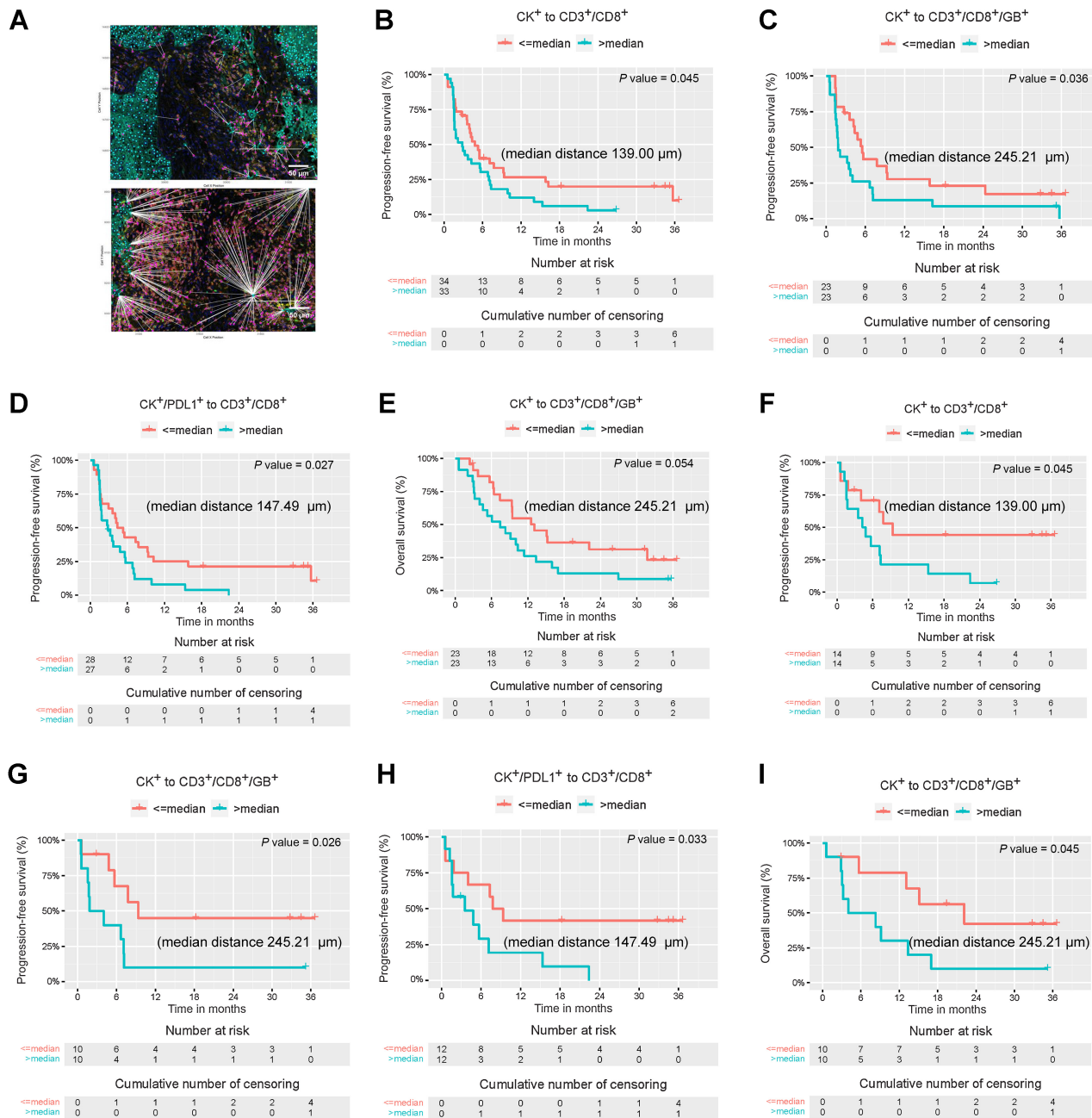
Blood-based biomarkers are attractive because they are non-invasive, dynamic, and less impacted by intratumor heterogeneity

than tissue-based markers (47). We performed Olink proximity extension assay using the immuno-oncology panel assaying a series of 92 proteins in 561 serum samples collected longitudinally from 160 patients. Using mixed models to account for demographic and relevant clinical covariates with multiple testing adjustments, several serum chemokines (CXCL9, CXCL10, CXCL13, CCL19) and activated T-cell markers (PD-1, IFN γ , IL12, IL10) were found durably increased from baseline with either nivo or nivo+ipi, (Fig. 4A and B) indicating the ICIs' immune regulating effect. Multiple markers of immune activation and priming (ICOS-L, LAMP3/DC-LAMP, IL4, IL13, NRC1, CD5) were found increased at baseline or early during treatment in responders, regardless of treatment type ($P < 0.05$; Fig. 4C and D), in line with associations of these important immune processes with clinical response to ICI. Conversely, macrophage-derived and hyperinflammation markers, such as IL6, IL8, CXCL13, CSF-1, TNFSF14/LIGHT, and CCL23, as well as likely stromal or tumor-derived markers, such as VEGFA, HGF, and HO-1, were significantly upregulated in nonresponders at baseline or after ICI preceding radiologic progression, with some differences based on treatment received for CXCL13 and CSF-1 ($P < 0.05$; Fig. 4C and D). Joint modeling of survival with Olink analytes showed an increased risk of death (HR > 1) with higher longitudinal serum levels of CXCL13, MMP12, CSF-1, and IL8, which was confirmed with independent Kaplan-Meier analyses based on median protein levels at baseline (Fig. 4E). Similar results were generally observed in the subset of patients with extreme outcomes (exceptional responders and early progressors), where LAMP3/DC-LAMP was higher while CXCL13, CCL23, and TNFSF14 were lower in exceptional responders at baseline compared with nonresponders (Fig. 4F, $P < 0.05$). Together with the above-described data, and considering only baseline markers, these results suggest that an activated T-cell signature (cytotoxic effector T cells and DC-LAMP) was important for responsiveness to treatment with either nivo or nivo+ipi, while a hyperinflammatory milieu (IL6, IL8, CXCL13, CCL23, TNFSF14/LIGHT, CSF-1, MMP12) had an adverse impact on response and OS.

Integrative analysis of immune features across different platforms

The antitumor immunity and response to ICIs is often determined at different molecular levels. The multiomics profiling in this study provided a unique opportunity for integrative analysis to understand the molecular and immune features associated with ICI benefit. We first performed recursive partitioning on Olink, mIF, NanoString, and WES data for classification of responders (Supplementary Fig. S8A and S8B). We identified that proteins from Olink provide good prediction on response. However, mIF markers did not contribute significantly in the decision tree, which might be due to relatively small sample size for mIF ($n = 159$ for Olink and $n = 82$ for mIF). We next created a decision tree survival prediction model and observed that

(Continued.) Representative multispectral images of panels 1(B) and 2(C) show high levels of inflammatory cells in a sample from an exceptional responder patient. **D**, Box plot shows GZB+ CTLs (CD3+CD8+GZB+) in patients with exceptional response compared with patients with early progression/death. Representative multispectral images of panels 1(E) and 2(F) show reduced immune infiltration in a progression/death patient sample. **G**, The spatial organization of immune and malignant cell phenotypes for the two mIF panels is shown with an example each from exceptional responders and early progressors. The colors for the different subpopulations are indicated under panel phenotype legend (on the left). **H**, For the above images, segregation of different cell phenotypes based on their spatially varying probabilities is shown as a contour plot. The colors of different neighborhoods are same as the panel phenotypes (above). **I**, For the above images, Euclidean distance-based clusters of cells (10 or more) within 20 μ m are identified. The clusters are represented by numbers and distinct colors. **J**, The relative percentage composition of cell types within each cluster (above) is indicated in the heat map. The corresponding cluster colors are indicated below the heat map for reference. The color scale representing percentage composition (0–100) is shown on the left.

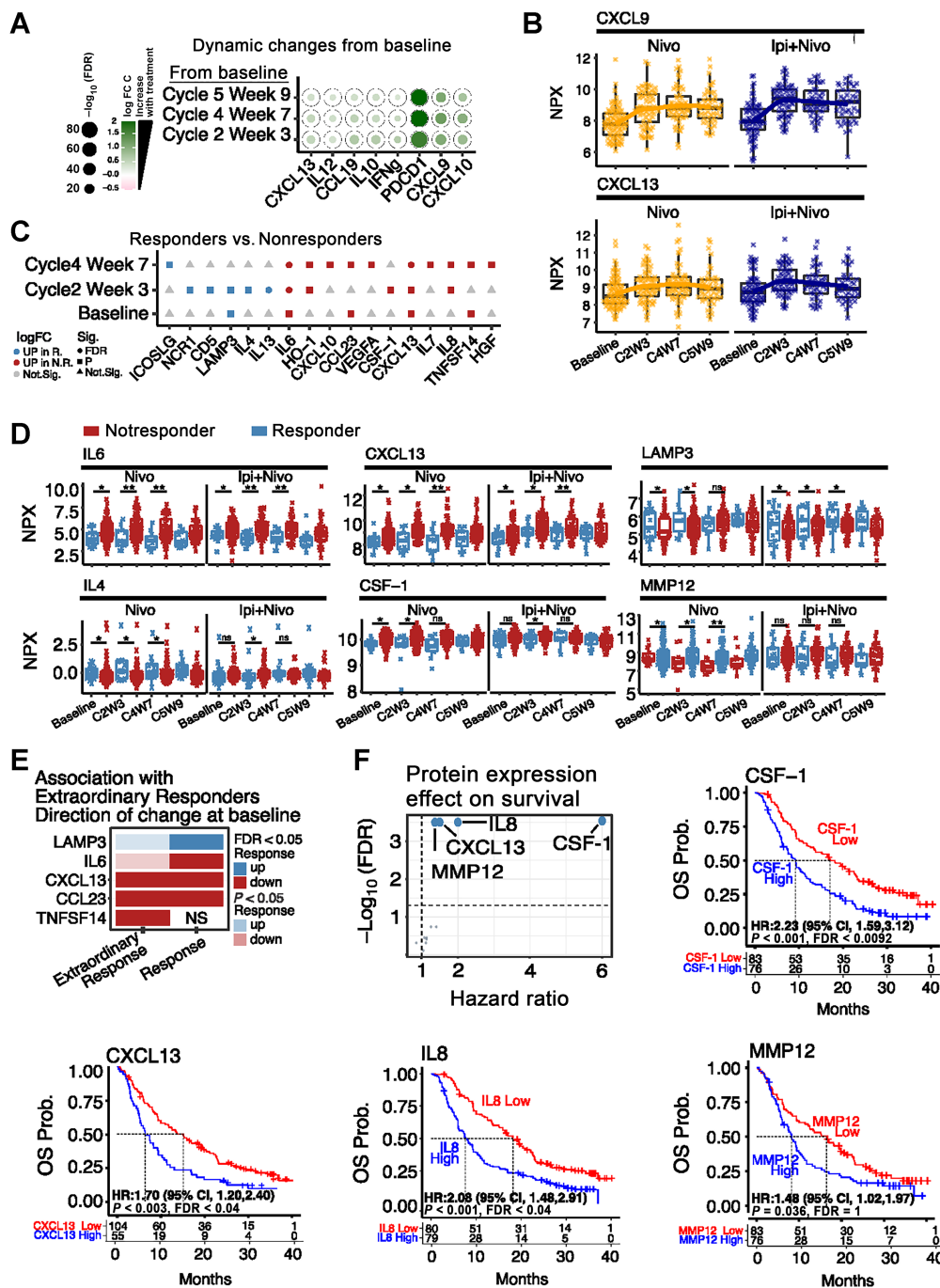
**Figure 3.**

Kaplan-Meier survival curves of nearest neighbor distance from both arms. **A**, Upper and lower image showing proximity map overlay, where cyan dots represent malignant cells (CK+) and red dots represent T cells (CD3+). White lines display distances from all malignant cells (CK+) to neighboring T cells (CD3+). Kaplan-Meier survival curves show that distances (\leq the median value used as cutoff) from malignant cells (CK+) to CTLs (CD3+CD8+; **B**) and GZB+ CTLs (CD3+CD8+GZB+; **C**), and malignant cells expressing PD-L1 (CK+PD-L1+) to CTLs (CD3+CD8+; **D**) were associated with better PFS when combining both treatment arms. **E**, Kaplan-Meier OS curve for distances from malignant (CK+) to GZB+ CTLs (CD3+CD8+GZB+) in both arms. In the nivo+ipi arm, Kaplan-Meier survival curves show that close distances (\leq the median value used as cutoff) from malignant cells (CK+) to CTLs (CD3+CD8+; **F**) and GZB+ CTLs (CD3+CD8+GZB+; **G**), and PD-L1+ malignant cells (CK+PD-L1+) to CTLs (CD3+CD8+; **H**) were associated with better PFS. **I**, Close distances from malignant cells (CK+) to GZB+ CTLs (CD3+CD8+GZB+) was associated with OS.

567 Cytotoxic.T.cells.antigen.experienced (CD3+CD8+PD-1+) together
568 with IL6, LAG3 and MICA.B separate patients into sub-populations
569 with different survival. Furthermore, we applied random forest
570 classifier, which identified Cytotoxic.T.cells.antigen.experienced

(CD3+CD8+PD-1+) and IL6 as important variables. NanoString and WES did not contribute to the association between omics markers and outcomes likely due to insufficient samples with data from these platforms.

572
573
574
575

**Figure 4.**

Olink serum soluble analyte assessment. **A**, Heat map of dynamic changes in protein expression. The x-axis shows the protein names, while the y-axis shows the comparisons between timepoints and progression. The color represents the logFC. Green represents increase from baseline while pink represents decrease. The size of the circle indicates the statistical significance expressed as $-\log_{10}(\text{FDR})$. **B**, Boxplots and median rend lines showing the expression over time by cohort for CXCL9 and CXCL13. **C**, Heat map for differential protein expression between responders and nonresponders. The x-axis shows the protein names, while the y-axis shows each timepoint. The symbol in the heat map represents the statistical significance: circles for $\text{FDR} < 0.05$ or adjusted P values, squares for $P < 0.05$, and triangles for nonsignificant or $P > 0.05$. The color represents the change relative to upregulation in responders (blue) or nonresponders (red). **D**, Boxplots corresponding to significant markers in **C** over time, stratified by treatment arm for the indicated proteins. Comparisons for individual baseline, cycle 2, and cycle 4 timepoints are shown for $P < 0.05$ and $\text{FDR} < 0.05$ with (*) and (**), respectively. **E**, Heat map showing the concordance in directionality of differentially expressed proteins significant between exceptional responders and all responders. The direction of the protein changes was identical between both groups of responders, but only CXCL13 and CCL23 reached statistical significance (FDR, darker colors) for exceptional responders due to the decreased numbers. Nominal significance is shown as transparent colors, indicating proteins with $P < 0.05$. **F**, Volcano plot showing the proteins significantly associated with OS when jointly modeling cytokine expression over time. The proteins labeled in blue are associated with increased HR or decreased survival. Kaplan–Meier OS curves for CSF-1, IL8, CXCL13, and MMP12 stratified on the basis of their expression from the average expression (higher values from the mean as blue, lower values from the mean as red).

578 **Discussion**

579 Identifying novel biomarkers for ICI response is challenging
 580 because the molecular determination of TME and host immune
 581 response is complex and heterogeneous across different patients. A
 582 large sample size to control interpatient heterogeneity and multi-omics
 583 to identify the determinates at different molecular levels are ideal but
 584 challenging. Therefore, maximizing the use of clinical, pathologic,
 585 molecular data and learning from each patient, particularly from
 586 clinical trials and careful analysis is key to pave the way to advance
 587 our understanding and ultimately the efficacy of ICI.

588 In this study, we performed mIF, gene expression profiling, WES,
 589 and OLINK on the previous samples from S1400I and identified
 590 known and novel molecular features associated with nivo versus
 591 nivo+ipi combination. Responders demonstrated higher densities of
 592 multiple immune cell types defined by mIF. Analysis of CTL populations
 593 revealed that GZB+ CTLs (CD3+CD8+GZB+) located in the
 594 tumor compartment were associated with better PFS. This was cor-
 595 roborated by analyzing the spatial organization of cell phenotypes,
 596 whereas higher immune cell population in the tumor region was seen
 597 in the TME of exceptional responders than that of early progressors.
 598 On the other hand, higher densities of Tregs (CD3+CD8-FOXP3+)
 599 in the total compartment correlated with worse OS in the nivo+ipi
 600 arm. This highlights the emerging dichotomy regarding the impact of
 601 ICI therapies on Treg subsets and function (48), as these combinations
 602 may not modulate some Treg subsets and dominance of CTLs is
 603 needed to overcome local immune suppression. Conversely, higher
 604 densities of memory T cells (CD3+CD45RO+) and Treg/memory T
 605 cells (CD3+CD8-CD45RO+FOXP3+) were associated with better
 606 PFS in the nivo arm. As PD-1 targeting has been shown to result in the
 607 reactivation of T cells already present within the tumor immune
 608 microenvironment, the presence of Treg/memory T cells at baseline
 609 may be an essential biomarker to delineate the need for inclusion of
 610 ipilimumab as opposed to a nivolumab alone approach. Estimating the
 611 immune subsets using TIMER and nSolver software demonstrated that
 612 a higher immune presence was associated with improved outcome.
 613 These results emphasize that an active immune response within the
 614 TME is required for a favorable clinical outcome in this setting, which
 615 is supported by multiple findings identifying mechanisms of response
 616 to ICI-based therapeutic strategies across various cancer types (49-51).

617 The TME is composed of various immune cells and stroma cells
 618 entangled with cancer cells. In addition to the densities of different
 619 cells, the spatial distribution and proximity among various cell types
 620 are also essential features with important impact on the functional
 621 status of the tumor immune microenvironment (52, 53). mIF data
 622 from this study provided an opportunity to assess the spatial rela-
 623 tionship of different cellular components within the tumor immune
 624 microenvironment and their association with clinical outcomes from
 625 ICI treatment. Using the spatial point metrics through the nearest
 626 neighbor analysis, we observed that tumors with higher densities of
 627 GZB+ CTLs close to malignant cells were associated with better PFS
 628 and OS in the nivo+ipi arm, suggesting that cell-to-cell distribution
 629 and specially CTLs play an important role in response to ICIs as
 630 showed by others studies in NSCLC (54). The organization of cells into
 631 clusters based on distance also demonstrated that the CTLs and
 632 malignant cells cluster more frequently in exceptional responders
 633 than early progressors suggesting a preformed antitumor response
 634 that is aided by the ICI.

635 We used WES to identify genomic features underlying particular
 636 immune features and found that a higher CNV burden was associated
 637 with a lower level of immune cell infiltration overall. Similarly, CNV

burden was negatively associated with immune scores derived from
 638 immune gene expression profiling. These findings are in line with
 639 previous findings in different cancer types suggesting that chromo-
 640 somal instability may be a common genomic alteration underlying
 641 immune evasion across human malignancies (53, 55-58). Interestingly,
 642 we also found that patients with *LRP1B*-mutant tumors had a
 643 reduced survival compared with patients without *LRP1B* mutations.
 644 *LRP1B* has been identified as a putative tumor suppressor and is
 645 frequently inactivated in NSCLCs (45). Recently, *LRP1B* mutation was
 646 reported to be associated with better prognosis in melanoma and
 647 NSCLC after anti-PD-1 therapy (46). However, in our cohort, we
 648 observed that *LRP1B* mutation was associated with a worse OS and PFS
 649 in both the nivo arm and nivo+ipi combination therapy arms. It is still
 650 unclear whether the difference was due to different histology (predomi-
 651 nantly adenocarcinoma in the previous study vs. exclusively
 652 squamous cell carcinoma in the current study) or different ICI
 653 (anti-PD-1 vs. anti-PD-1 with/without anti-CTLA-4) or low sample
 654 size. Of note, the impact of *LRP1B* mutations on cancer biology and
 655 response to ICIs has not been clearly defined in different cancers. For
 656 example, a study on renal clear-cell carcinoma reported worse pro-
 657 gnosis and suppressive antitumor immunity when *LRP1B* was over-
 658 expressed (59), and another found that *LRP1B* mutations were asso-
 659 ciated with inferior clinical outcomes after ICI treatment in patients
 660 with hepatocellular carcinoma (60).

661 Although tissue-based assays remain the gold standard for molec-
 662 ular profiling for oncology practice, liquid biopsy, particularly peripher-
 663 al blood-based assays, have gained more attention for molecular
 664 profiling and disease monitoring across various cancers because they
 665 are noninvasive, "real-time," and less affected by intratumor hetero-
 666 geneity (61, 62). In the era of immune-oncology, the Olink soluble
 667 protein detection platform has emerged as a promising tool to assess
 668 and monitor host immune response. Using Olink, we identified a high
 669 level of protumorigenic factors, such as VEGFA and CCL23, and
 670 inflammatory markers, such as IL6, IL8, and MMP12, that were
 671 associated with inferior survival in this cohort of patients. These
 672 findings suggest that general inflammation is detrimental in the
 673 context of cancer and ICI therapy. In contrast, proteins involved in
 674 T-cell and natural killer cell activation, such as LAMP3/DC-LAMP,
 675 IFN γ /IL4/IL13, and NRC-1, were associated with improved outcomes
 676 after ICI therapy. It was unexpected that a high level of CXCL13 was
 677 associated with poor response to ICI therapy and shorter survival,
 678 given the recent studies reporting this chemokine working together
 679 with DC-LAMP and playing essential roles in the establishment of
 680 tertiary lymphoid structures in NSCLC (63). It is possible that the
 681 relatively high levels of circulating CXCL13 in the serum do not reflect
 682 relatively rare CD4 $^{+}$ T cell-derived tumor tissue-specific expression of
 683 CXCL13, and this emphasizes the limitations of soluble analytes as a
 684 surrogate for local tumor events. Some analytes, such as CXCL9/10 and
 685 soluble PD-1, were dynamically increased with treatment and mar-
 686 ginally associated with outcomes in exceptional responders, in line
 687 with previous reports (64). Of particular interest, other markers
 688 showed the strongest association with objective response during ICI
 689 treatment, for example, lower CSF-1 or IL6 or higher IL13 at cycle 2.
 690 This is reminiscent of findings from melanoma studies in which the
 691 on-treatment biopsy was more informative for long-term benefit from
 692 ICIs than the baseline biopsy, as the actual changes after treatment
 693 reflect the host immune system's response to ICIs more accurately
 694 (65, 66). Although soluble analytes are not ideal predictive biomar-
 695 kers to select an optimal initial treatment regimen, if validated, these
 696 markers will be extremely helpful in switching ineffective therapy to
 697 effective alternatives to save time and potential toxicity, which is
 698 699

critically important for patients with stage IV lung cancers, for whom time and quality of life are essential attributes. In addition, these on-treatment markers are also valuable in distinguishing pseudoprogression from real progression—another critical clinical dilemma that the oncologists face in the era of immuno-oncology.

As a *post hoc* profiling of samples from a completed clinical trial, our study has several inherent limitations, including inadequate tumor specimen availability, which precluded us from generating comprehensive data integration from all platforms; imbalanced distribution of samples from the nivo versus nivo+ipi arms or responders versus nonresponders; inadequate tissues for multiomic analysis and cross-platform integrative analyses; and lack of detailed information regarding the time and anatomic sites of tumor specimens, which limited our ability to perform in-depth, organ-specific analysis. In spite of these challenges, integration of peripheral cytokine profiling and cellular profiling within the TME confirmed our single platform findings highlighting the negative association with hyperinflammation with reduced PFS and the presence of PD-1+ CTLs in the TME with increased survival. Finally, while we presented several candidates in this study, we recognize the need for additional validation and replication of our findings. Specifically, several circulating serum proteins, such as IL6, IL8, CSF-1, MMP12, and CXCL13 are promising candidates for future prospective or *post hoc* confirmatory studies due to their ease of collection and quantification from blood. In addition, investigation of tissue composition using spatial profiling technologies to better understand the complex interplay between tumor tissue and immune infiltrating cells may shed light on the mechanisms of immune-tumor cell-cell interactions and identify key biomarkers that can identify patients who will have the most benefit from ICIs. As a proof-of-principle study, using the S14001 trial as an example, we showcased that multi-omics, multi-institutional analyses of patient samples are feasible and can provide valuable insights for future trial development, which is one of the major goals of the CIMAC-CIDC Network.

Authors' Disclosures

D.Y. Duose reports grants from NIH during the conduct of the study; other support from Chrysalis Biomedical outside the submitted work; and Issued Patent Application No. 62/866,130 entitled "METHODS FOR DUPLEX SEQUENCING OF CELL-FREE DNA AND APPLICATIONS THEREOF". F. Michor is a co-founder of and has equity in Harbinger Health, has equity in Zephyr AI, and serves as a consultant for both companies. F. Michor is also on the board of directors of Exscientia Plc. F. Michor declares that none of these relationships are directly or indirectly related to the content of this article. J.E. Gray reports personal fees from AbbVie, Axiom HC Strategies, Blueprint Medicines, Celgene, Daiichi Sankyo, Inc, EMD Serono - Merck KGaA, Invivata, Janssen Scientific, Jazz Pharmaceuticals, Loxo Oncology Inc, OncoCyte Biotechnology, Sanofi Pharmaceuticals, and Takeda Pharmaceuticals; grants from Boehringer Ingelheim, G1 Therapeutics, Ludwig Institute of Cancer Research, Pfizer; grants and personal fees from AstraZeneca, Bristol Myers Squibb, Genentech, Merck & Co, Inc, Novartis outside the submitted work. R. Herbst reports other support from AstraZeneca personal fees and other support from Eli Lilly and Company; personal fees from Genentech/Roche and Merck and Company during the conduct of the study; personal fees from AbbVie Pharmaceuticals, Immunocore, Junshi Pharmaceuticals, Bristol Myers Squibb, Codel Therapeutics, Cybrexa Therapeutics, DynamisCure Biotechnology, eFFECTOR Therapeutics, EMD Serono, Gilead, HiberCell Inc, I-Mab Biopharma, Immune-Onc Therapeutics, Inc, Janssen, Johnson & Johnson, Loxo Oncology, Mirati Therapeutics, NextCure, Novartis, Ocean Biomedical, Inc, Oncocyte Corp, Oncternal Therapeutics, Pfizer, Regeneron Pharmaceuticals, Reveal Biotherapeutics, Inc, Ribbon Therapeutics, Sanofi, Seattle Genetics, and Xencor, Inc; other support from Bolt Biotherapeutics; personal fees and other support from Checkpoint Therapeutics, Normuity outside the submitted work; and board member: American Association for Cancer Research, International Association for the Study of Lung Cancer; committee member: Society for Immunotherapy of Cancer, Southwest Oncology Group. I.I. Wistuba reports grants and personal fees from Genentech/Roche, Bayer, Bristol Myers Squibb,

AstraZeneca, Pfizer, Merck, Guardant Health, Sanofi, Novartis, Sanofi, Novartis; personal fees from GlaxoSmithKline, Flame, Daiichi Sankyo, Jansen, Merus, Regeneron, Oncocyte, MSD; grants from Adaptive, Adaptimmune, EMD Serono, Karus, Johnson & Johnson, Iovance, 4D, and Akoya outside the submitted work. S. Gettinger reports grants from Bristol Myers Squibb outside the submitted work. K. Kelly reports other support from BMS during the conduct of the study. L. Bazhenova reports personal fees from Neuvogen, BioAtla, Summit therapeutics, Anheart, Gilead, Merck, Abbvie, Regeneron, Janssen, Genentech, Novocure, Intervenn, Elevation Oncology, ORIC, Mirati, Turning point, Daichi, Bayer, Sanofi, Novartis, BMS, and BI outside the submitted work. S. Gnatic reports grants from Regeneron, Boehringer-Ingelheim, Genentech, Takeda, BMS, Celgene, and Janssen R&D outside the submitted work. J. Zhang reports grants from Meck; grants and personal fees from Johnson & Johnson, Novartis; personal fees from Bristol Myers Squibb, AstraZeneca, GenePlus, Innoven, Hengrui, and Varian outside the submitted work. C. Haymaker reports grants from NCI during the conduct of the study; grants from Sanofi, Dragonfly, BTG, Trisalus, Iovance, Avenge, Obsidian; personal fees from Briacell, Nanobiotix, SWOG, and SITC outside the submitted work. No disclosures were reported by the other authors.

Q8 766
767
768
769
770
771
772
773
774
775
776
777
778
779
780
781
782

Authors' Contributions

E.R. Parra: Conceptualization, investigation, methodology, writing-original draft, writing-review and editing. J. Zhang: Formal analysis, methodology, writing-original draft, writing-review and editing. D.Y. Duose: Investigation, methodology, writing-original draft, writing-review and editing. E. Gonzalez-Kozlova: Investigation, visualization, methodology, writing-original draft, writing-review and editing. M.W. Redman: Formal analysis, investigation, writing-original draft, writing-review and editing. H. Chen: Formal analysis, investigation, methodology, writing-review and editing. G.C. Manyam: Formal analysis, investigation, methodology, writing-review and editing. G. Kumar: Visualization, methodology, writing-review and editing. J. Zhang: Investigation, methodology, writing-review and editing. X. Song: Investigation, methodology, writing-review and editing. R. Lazcano: Investigation, writing-review and editing. M.L. Marques-Piubelli: Investigation, writing-review and editing. C. Laberiano-Fernandez: Investigation, writing-review and editing. F. Rojas: Investigation, writing-review and editing. B. Zhang: Investigation, writing-review and editing. L. Taing: Investigation, methodology, writing-review and editing. A. Jhaveri: Investigation, methodology, writing-review and editing. J. Geisberg: Investigation, methodology, writing-review and editing. J. Altreuter: Resources, investigation, methodology, writing-review and editing. F. Michor: Resources, investigation, methodology, writing-review and editing. J. Provencher: Resources, investigation, methodology, writing-review and editing. J. Yu: Resources, investigation, methodology, writing-review and editing. E. Cerami: Resources, investigation, methodology, writing-review and editing. R. Moravec: Resources, writing-review and editing. K. Kannan: Investigation, methodology, writing-original draft, writing-review and editing. R. Luthra: Resources, investigation, writing-review and editing. G. Alatash: Funding acquisition, writing-original draft, writing-review and editing. H.-H. Huang: Investigation, methodology, writing-review and editing. H. Xie: Investigation, methodology, writing-review and editing. M. Patel: Investigation, methodology, writing-review and editing. K. Nie: Investigation, methodology, writing-review and editing. J. Harris: Investigation, methodology, writing-review and editing. K. Argueta: Investigation, methodology, writing-review and editing. J. Lindsay: Resources, investigation, methodology, writing-review and editing. R. Biswas: Resources, investigation, methodology, writing-review and editing. S. Van Nostrand: Investigation, methodology, writing-review and editing. S. Kim-Schulze: Resources, investigation, methodology, writing-review and editing. J.E. Gray: Investigation, writing-review and editing. R. Herbst: Investigation, writing-review and editing. I.I. Wistuba: Supervision, funding acquisition, writing-original draft, writing-review and editing. S. Gettinger: Investigation, writing-original draft, writing-review and editing. K. Kelly: Investigation, writing-original draft, writing-review and editing. L. Bazhenova: Investigation, writing-original draft, writing-review and editing. S. Gnatic: Supervision, writing-original draft, writing-review and editing. J.J. Lee: Data curation, formal analysis, supervision, validation, methodology, writing-original draft, writing-review and editing. J. Zhang: Conceptualization, supervision, investigation, writing-original draft, writing-review and editing. C. Haymaker: Conceptualization, supervision, funding acquisition, investigation, writing-original draft, writing-review and editing.

783
784
785
786
787
788
789
790
791
792
793
794
795
796
797
798
799
800
801
802
803
804
805
806
807
808
809
810
811
812
813
814
815
816
817
818
819
820
821
822
823
824
825
826
827
828
Q9 829

Acknowledgments

Scientific and financial support for the CIMAC-CIDC Network is provided through the NCI Cooperative Agreements U24CA224319 (to the Icahn School of

835	Medicine at Mount Sinai CIMAC), U24CA224285 (to MD Anderson Cancer Center 836 CIMAC) and U24CA224316 (to the CIDE at Dana-Farber Cancer Institute). SWOG 837 Study S1400I was supported in part by NIH/NCI grants U10CA180888 and 838 U10CA180819 and in part by Bristol Myers Squibb Company, through the Foundation 839 for the NIH, in partnership with Friends of Cancer Research. Scientific and 840 financial support for the Partnership for Accelerating Cancer Therapies (PACT) 841 public-private partnership (PPP) are made possible through funding support provided 842 to the FNIH by: AbbVie Inc., Amgen Inc., Boehringer-Ingelheim Pharma 843 GmbH & Co. KG, Bristol-Myers Squibb, Celgene Corporation, Genentech Inc, 844 Gilead, GlaxoSmithKline plc, Janssen Pharmaceutical Companies of Johnson & 845 Johnson, Novartis Institutes for Biomedical Research, Pfizer Inc., and Sanofi.	854
846	We thank the members of the Translational Molecular Pathology Immuno- 847 Profiling (TMP-II) MoonShots Platform at MD Anderson for their support. We 848 thank Beatriz Sanchez-Espiridion, Julia Mendoza Perez, Shani Wijeratne, and Celia 849 Garcia-Prieto for their assistance with sample procurement and inventory; Mei Jiang, 850 Auriola Tamegnon, Heladio Ibarguen, Salome McAllen, Saxon Rodriguez, Jianling 851 Zhou, Mauricio E Vasquez Juarez, and Renganayaki Krishna Pandurengan for their 852 technical assistance; Dawen Sui and Juan Ruiz Posadas for data transfer; and Curtis	855
856	Gumbs and Latasha Little for genomics support. Seunghee Kim-Schulze, for his help 857 in running Olink assays. We thank Diane Del Valle for project management from the 858 Mt. Sinai CIMAC, Magdalena Thurin, Helen Chen, Minkyung Song from NCI and 859 Rebecca Enos from Emmes. Editorial support was provided by Bryan Tutt, Scientific 860 Editor, Research Medical Library at MD Anderson Cancer Center. We thank the 861 patients and their families for participating in the study.	859
860	The publication costs of this article were defrayed in part by the payment of 861 publication fees. Therefore, and solely to indicate this fact, this article is hereby 862 marked "advertisement" in accordance with 18 USC section 1734.	860
863	Note	863
864	Supplementary data for this article are available at Clinical Cancer Research Online (http://clincancerres.aacrjournals.org/).	864
865	Received January 31, 2023; revised May 6, 2023; accepted January 24, 2024; published first January 26, 2024.	865
866		866
867		867

References

1. Topalian SL, Hodi FS, Brahmer JR, Gettinger SN, Smith DC, McDermott DF, et al. Safety, activity, and immune correlates of anti-PD-1 antibody in cancer. *N Engl J Med* 2012;366:2443–54.
2. Brahmer J, Reckamp KL, Baas P, Crino L, Eberhardt WE, Poddubskaya E, et al. Nivolumab versus docetaxel in advanced squamous-cell non-small-cell lung cancer. *N Engl J Med* 2015;373:123–35.
3. Herbst RS, Baas P, Kim DW, Felip E, Perez-Gracia JL, Han JY, et al. Pembrolizumab versus docetaxel for previously treated, PD-L1-positive, advanced non-small-cell lung cancer (KEYNOTE-010): a randomised controlled trial. *Lancet* 2016;387:1540–50.
4. Fehrenbacher L, von Pawel J, Park K, Rittmeyer A, Gandara DR, Ponce Aix S, et al. Updated efficacy analysis including secondary population results for OAK: a randomized phase III study of atezolizumab versus docetaxel in patients with previously treated advanced non-small cell lung cancer. *J Thorac Oncol* 2018;13: 1156–70.
5. Paz-Ares L, Luft A, Vicente D, Tafreshi A, Gumus M, Mazieres J, et al. Pembrolizumab plus chemotherapy for squamous non-small-cell lung cancer. *N Engl J Med* 2018;379:2040–51.
6. West H, McCleod M, Hussein M, Morabito A, Rittmeyer A, Conter HJ, et al. Atezolizumab in combination with carboplatin plus nab-paclitaxel chemotherapy compared with chemotherapy alone as first-line treatment for metastatic non-squamous non-small-cell lung cancer (IMpower130): a multicentre, randomised, open-label, phase 3 trial. *Lancet Oncol* 2019;20:924–37.
7. Hellmann MD, Paz-Ares L, Bernabe Caro R, Zurawski B, Kim SW, Carcereny Costa E, et al. Nivolumab plus ipilimumab in advanced non-small-cell lung cancer. *N Engl J Med* 2019;381:2020–31.
8. Paz-Ares L, Ciuleanu TE, Cobo M, Schenker M, Zurawski B, Menezes J, et al. First-line nivolumab plus ipilimumab combined with two cycles of chemotherapy in patients with non-small-cell lung cancer (CheckMate 9LA): an international, randomised, open-label, phase 3 trial. *Lancet Oncol* 2021;22:198–211.
9. Li F, Dong X. Pembrolizumab provides long-term survival benefits in advanced non-small cell lung cancer: the 5-year outcomes of the KEYNOTE-024 trial. *Thorac Cancer* 2021;12:3085–7.
10. Jassem J, de Marinis F, Giaccone G, Vergnenegre A, Barrios CH, Morise M, et al. Updated overall survival analysis from IMpower110: atezolizumab versus platinum-based chemotherapy in treatment-naïve programmed death-ligand 1-selected NSCLC. *J Thorac Oncol* 2021;16:1872–82.
11. Neoadjuvant PD-1 blockade in resectable lung cancer; Nivolumab and ipilimumab in advanced melanoma; overall survival with combined nivolumab and ipilimumab in advanced melanoma; prolonged survival in stage III melanoma with ipilimumab adjuvant therapy; combined nivolumab and ipilimumab or monotherapy in untreated melanoma; combined nivolumab and ipilimumab or monotherapy in untreated melanoma; nivolumab and ipilimumab versus ipilimumab in untreated melanoma; rapid eradication of a bulky melanoma mass with one dose of immunotherapy; genetic basis for clinical response to CTLA-4 blockade; genetic basis for clinical response to CTLA-4 blockade in melanoma; nivolumab plus ipilimumab in advanced melanoma; safety and tumor responses with lambrolizumab (Anti-PD-1) in melanoma; hepatotoxicity with combination of vemurafenib and ipilimumab. *N Engl J Med* 2018;379:2185.
12. Wolchok JD, Chiarion-Sileni V, Gonzalez R, Rutkowski P, Grob JJ, Cowey CL, et al. Overall survival with combined nivolumab and ipilimumab in advanced melanoma. *N Engl J Med* 2017;377:1345–56.
13. Ready N, Hellmann MD, Awad MM, Otterson GA, Gutierrez M, Gainor JF, et al. First-line nivolumab plus ipilimumab in advanced non-small-cell lung cancer (checkmate 568): outcomes by programmed death ligand 1 and tumor mutational burden as biomarkers. *J Clin Oncol* 2019;37:992–1000.
14. Hellmann MD, Rizvi NA, Goldman JW, Gettinger SN, Borghaei H, Brahmer JR, et al. Nivolumab plus ipilimumab as first-line treatment for advanced non-small-cell lung cancer (CheckMate 012): results of an open-label, phase 1, multicohort study. *Lancet Oncol* 2017;18:31–41.
15. Gettinger SN, Redman MW, Bazhenova L, Hirsch FR, Mack PC, Schwartz LH, et al. Nivolumab plus ipilimumab vs nivolumab for previously treated patients with stage IV squamous cell lung cancer: the lung-MAP S1400I phase 3 randomized clinical trial. *JAMA Oncol* 2021;7:1368–77.
16. Hong L, Negrao MV, Dibaj SS, Chen R, Reuben A, Bohac JM, et al. Programmed death-ligand 1 heterogeneity and its impact on benefit from immune checkpoint inhibitors in NSCLC. *J Thorac Oncol* 2020;15:1449–59.
17. Herbst RS, Soria JC, Kowanetz M, Fine GD, Hamid O, Gordon MS, et al. Predictive correlates of response to the anti-PD-L1 antibody MPDL3280A in cancer patients. *Nature* 2014;515:563–7.
18. Klempner SJ, Fabrizio D, Bane S, Reinhart M, Peoples T, Ali SM, et al. Tumor mutational burden as a predictive biomarker for response to immune checkpoint inhibitors: a review of current evidence. *Oncologist* 2020;25:e147–e59.
19. Hellmann MD, Nathanson T, Rizvi H, Creelan BC, Sanchez-Vega F, Ahuja A, et al. Genomic features of response to combination immunotherapy in patients with advanced non-small-cell lung cancer. *Cancer Cell* 2018;33: 843–52.
20. Parra ER, Ferrufino-Schmidt MC, Tamegnon A, Zhang J, Solis L, Jiang M, et al. Immuno-profiling and cellular spatial analysis using five immune oncology multiplex immunofluorescence panels for paraffin tumor tissue. *Sci Rep* 2021;11: 8511.
21. Parra ER, Jiang M, Solis L, Mino B, Laberiano C, Hernandez S, et al. Procedural requirements and recommendations for multiplex immunofluorescence tyramide signal amplification assays to support translational oncology studies. *Cancers* 2020;12:255.
22. Baddeley A, Turner R. spatstat: an R package for analyzing spatial point patterns. *J Stat Softw* 2005;12:1–42.
23. Waggett D, Chu K, Yin S, Wouters BG, Liu FF, Boutros PC. NanoStringNorm: an extensible R package for the pre-processing of NanoString mRNA and miRNA data. *Bioinformatics* 2012;28:1546–8.
24. McKenna A, Hanna M, Banks E, Sivachenko A, Cibulskis K, Kernytsky A, et al. The genome analysis toolkit: a mapreduce framework for analyzing next-generation DNA sequencing data. *Genome Res* 2010;20:1297–303.
25. Kendig KI, Baheti S, Bockol MA, Drucker TM, Hart SN, Heldenbrand JR, et al. Senteon DNASeq variant calling workflow demonstrates strong computational performance and accuracy. *Front Genet* 2019;10:736.
26. McLaren W, Gil L, Hunt SE, Riat HS, Ritchie GR, Thormann A, et al. The ensembl variant effect predictor. *Genome Biol* 2016;17:122.

- 970 27. Talevich E, Shain AH, Botton T, Bastian BC. CNVkit: genome-wide copy
971 number detection and visualization from targeted DNA sequencing.
972 PLoS Comput Biol 2016;12:e1004873.
973 28. Favero F, Joshi T, Marquard AM, Birkbak NJ, Krzstanek M, Li Q, et al.
974 Sequenza: allele-specific copy number and mutation profiles from tumor
975 sequencing data. Ann Oncol 2015;26:64–70.
976 29. Shen R, Seshan VE. FACETS: allele-specific copy number and clonal heterogeneity
977 analysis tool for high-throughput DNA sequencing. Nucleic Acids Res
978 2016;44:e131.
979 30. Gillis S, Roth A. PyClone-VI: scalable inference of clonal population structures
980 using whole genome data. BMC Bioinformatics 2020;21:571.
981 31. Roth A, Khattri J, Yap D, Wan A, Laks E, Biele J, et al. PyClone: statistical
982 inference of clonal population structure in cancer. Nat Methods 2014;11:396–8.
983 32. Monjazeb AM, Giobbie-Hurder A, Lako A, Thrash EM, Brennick RC, Kao KZ,
984 et al. Correction: a randomized trial of combined PD-L1 and CTLA-4 inhibition
985 with targeted low-dose or hypofractionated radiation for patients with metastatic
986 colorectal cancer. Clin Cancer Res 2021;27:4940.
987 33. Therneau TM, Grambsch PM. Modeling survival data: extending the Cox model.
988 New York: Springer; 2000.
989 34. Benjamini Y, Cohen R. Weighted false discovery rate controlling procedures for
990 clinical trials. Biostatistics 2017;18:91–104.
991 35. Hoffman GE, Roussos P. Dream: powerful differential expression analysis for
992 repeated measures designs. Bioinformatics 2021;37:192–201.
993 36. Bates D, Mächler M, Bolker B, Walker S. Fitting linear mixed-effects models
994 using lme4. J Stat Softw 2015;67:1–48.
995 37. Makowski D, Ben-Shachar M, Lüdecke D. bayestestR: describing effects and their
996 uncertainty, existence and significance within the bayesian framework. J Open
997 Source Software 2019;4:1581.
998 38. Gelman A, Rubin DB. Inference from iterative simulation using multiple
999 sequences. Sci Rep 1992;7:457–72.
1000 39. Flegal JM, Haran M, Jones GL. Markov chain Monte Carlo: can we trust the third
1001 significant figure? Stat Sci 2008;23:250–60.
1002 40. Rizopoulos D, Hatfield L, Carlin B, Takkenberg J. Combining dynamic predictions
1003 from joint models for longitudinal and time-to-event data using bayesian
1004 model averaging. J Am Statist Assoc 2014;109:1385–97.
1005 41. Wang H, Li G. A selective review on random survival forests for high dimensional
1006 data. Quant Biosci 2017;36:85–96.
1007 42. Ishwaran H, Kogalur UB, Blackstone EH, Lauer MS. Random survival forests.
1008 Ann Appl Stat 2008;2:841–60.
1009 43. Chen PL, Roh W, Reuben A, Cooper ZA, Spencer CN, Prieto PA, et al. Analysis of
1010 immune signatures in longitudinal tumor samples yields insight into biomarkers
1011 of response and mechanisms of resistance to immune checkpoint blockade.
1012 Cancer Discov 2016;6:827–37.
1013 44. Carstens JL, Correa de Sampaio P, Yang D, Barua S, Wang H, Rao A, et al. Spatial
1014 computation of intratumoral T cells correlates with survival of patients with
1015 pancreatic cancer. Nat Commun 2017;8:15095.
1016 45. Liu CX, Musco S, Lisitsina NM, Forgacs E, Minna JD, Lisitsyn NA. LRP-DIT, a
1017 putative endocytic receptor gene, is frequently inactivated in non-small cell lung
1018 cancer cell lines. Cancer Res 2000;60:1961–7.
1019 46. Chen H, Chong W, Wu Q, Yao Y, Mao M, Wang X. Corrigendum: association of
1020 LRP1B mutation with tumor mutation burden and outcomes in melanoma and
1021 non-small cell lung cancer patients treated with immune check-point blockades.
1022 Front Immunol 2019;10:1523.
1023 47. Lam VK, Zhang J. Blood-based tumor mutation burden: continued progress
1024 toward personalizing immunotherapy in non-small cell lung cancer. J Thorac
1025 Dis 2019;11:2208–11.
1026 48. Hui E, Cheung J, Zhu J, Su X, Taylor MJ, Wallweber HA, et al. T cell
1027 costimulatory receptor CD28 is a primary target for PD-1-mediated inhibition.
1028 Science 2017;355:1428–33.
49. Cristescu R, Mogg R, Ayers M, Albright A, Murphy E, Yearley J, et al. Pan-tumor
genomic biomarkers for PD-1 checkpoint blockade-based immunotherapy.
Science 2018;362;eaar3593.
50. Hsu CL, Ou DL, Bai LY, Chen CW, Lin L, Huang SF, et al. Exploring markers of
exhausted CD8 T cells to predict response to immune checkpoint inhibitor
therapy for hepatocellular carcinoma. Liver Cancer 2021;10:346–59.
51. Miller BC, Sen DR, Al Abosy R, Bi K, Virkud YV, LaFleur MW, et al. Subsets of
exhausted CD8(+) T cells differentially mediate tumor control and respond to
checkpoint blockade. Nat Immunol 2019;20:326–36.
52. Reuben A, Gittelman R, Gao J, Zhang J, Yusko EC, Wu CJ, et al. TCR repertoire
intratumor heterogeneity in localized lung adenocarcinomas: an association with
predicted neoantigen heterogeneity and postsurgical recurrence. Cancer Discov
2017;7:1088–97.
53. Chen R, Lee WC, Fujimoto J, Li J, Hu X, Mehran R, et al. Evolution of genomic
and T-cell repertoire heterogeneity of malignant pleural mesothelioma under
dasatinib treatment. Clin Cancer Res 2020;26:5477–86.
54. Bocchialini G, Lagrasta C, Madeddu D, Mazzaschi G, Marturano D, Sogni F, et al.
Spatial architecture of tumour-infiltrating lymphocytes as a prognostic parameter
in resected non-small-cell lung cancer. Eur J Cardiothorac Surg 2020;58:
619–28.
55. Hu X, Fujimoto J, Ying L, Fukuoka J, Ashizawa K, Sun W, et al. Multi-region
exome sequencing reveals genomic evolution from preneoplasia to lung ade-
nocarcinoma. Nat Commun 2019;10:2978.
56. Chen M, Chen R, Jin Y, Li J, Hu X, Zhang J, et al. Cold and heterogeneous T cell
repertoire is associated with copy number aberrations and loss of immune genes
in small-cell lung cancer. Nat Commun 2021;12:6655.
57. Dejima H, Hu X, Chen R, Zhang J, Fujimoto J, Parra ER, et al. Immune evolution
from preneoplasia to invasive lung adenocarcinomas and underlying molecular
features. Nat Commun 2021;12:2722.
58. Lee WC, Reuben A, Hu X, McGranahan N, Chen R, Jalali A, et al. Multiomics
profiling of primary lung cancers and distant metastases reveals immunosup-
pression as a common characteristic of tumor cells with metastatic plasticity.
Genome Biol 2020;21:271.
59. Feng C, Ding G, Ding Q, Wen H. Overexpression of low density lipoprotein
receptor-related protein 1 (LRP1) is associated with worsened prognosis and
decreased cancer immunity in clear-cell renal cell carcinoma. Biochem Biophys
Res Commun 2018;503:1537–43.
60. Wang M, Xiong Z. The mutation and expression level of LRP1B are associated
with immune infiltration and prognosis in hepatocellular carcinoma. Int J Gen
Med 2021;14:6343–58.
61. Nong J, Gong Y, Guan Y, Yi X, Yi Y, Chang L, et al. Author Correction:
Circulating tumor DNA analysis depicts subclonal architecture and genomic
evolution of small cell lung cancer. Nat Commun 2019;10:552.
62. Ma F, Guan Y, Yi Z, Chang L, Li Q, Chen S, et al. Assessing tumor heterogeneity
using ctDNA to predict and monitor therapeutic response in metastatic breast
cancer. Int J Cancer 2020;146:1359–68.
63. Leader AM, Grout JA, Maier BB, Nabey BY, Park MD, Tabachnikova A, et al.
Single-cell analysis of human non-small cell lung cancer lesions refines tumor
classification and patient stratification. Cancer Cell 2021;39:1594–609.
64. House IG, Savas P, Lai J, Chen AXY, Oliver AJ, Teo ZL, et al. Macrophage-
derived CXCL9 and CXCL10 are required for antitumor immune responses
following immune checkpoint blockade. Clin Cancer Res 2020;26:487–504.
65. Im SJ, Hashimoto M, Gerner MY, Lee J, Kissick HT, Burger MC, et al. Defining
CD8+ T cells that provide the proliferative burst after PD-1 therapy. Nature
2016;537:417–21.
66. Siddiqui I, Schaeuble K, Chennupati V, Fuertes Marraco SA, Calderon-Cope S,
Pais Ferreira D, et al. Intratumoral Tcf1(+)PD-1(+)CD8(+) T cells with stem-
like properties promote tumor control in response to vaccination and checkpoint
blockade immunotherapy. Immunity 2019;50:195–211.

AUTHOR QUERIES

AUTHOR PLEASE ANSWER ALL QUERIES

- Q1: Page: 1: Author: Per journal style, genes, alleles, loci, and oncogenes are italicized; proteins are roman. Please check throughout to see that the words are styled correctly. AACR journals have developed explicit instructions about reporting results from experiments involving the use of animal models as well as the use of approved gene and protein nomenclature at their first mention in the manuscript. Please review the instructions at <http://aacrjournals.org/content/authors/editorial-policies#genenomen> to ensure that your article is in compliance. If your article is not in compliance, please make the appropriate changes in your proof.
- Q2: Page: 1: Author: Please verify the drug names and their dosages used in the article.
- Q3: Page: 1: Author: Please verify the affiliations and their corresponding author links.
- Q4: Page: 1: Author: Please verify the corresponding author details.
- Q5: Page: 1: Author: Please note that the abbreviation "SqNSCLC" has been defined as "metastatic lung squamous cell carcinoma" in Abstract and "squamous NSCLC" in the text. Please retain the single spelled out form.
- Q6: Page: 5: Author: Please verify the layout of Tables for correctness.
- Q7: Page: 6: Author: Please confirm quality/labeling of all images included within this article. Figure labels should be legible at 100% zoom of the PDF file to ensure readability in print. Please flag any figures and/or label font sizes that should be adjusted.
- Q8: Page: 12: Author: The Authors' Disclosures statement that appears in the proof incorporates the information from forms completed and signed off on by each individual author. No factual changes can be made to disclosure information at the proof stage. However, typographical errors or misspelling of author names should be noted on the proof and will be corrected before publication. Please note if any such errors need to be corrected. Is the disclosure statement correct?
- Q9: Page: 12: Author: The contribution(s) of each author are listed in the proof under the heading "Authors' Contributions." These contributions are derived from forms completed and signed off on by each individual author. If you make changes to these contributions, you must inform the affected author(s).

AU: Below is a summary of the name segmentation for the authors according to our records. The First Name and the Surname data will be provided to PubMed when the article is indexed for searching. Please check each name carefully and verify that the First Name and Surname are correct. If a name is not segmented correctly, please write the correct First Name and Surname on this page and return it with your proofs. If no changes are made to this list, we will assume

that the names are segmented correctly, and the names will be indexed as is by PubMed and other indexing services.

First Name	Surname		
Edwin Roger	Parra	Kasthuri	Kannan
Jiexin	Zhang	Rajyalakshmi	Luthra
Dzifa Yawa	Duose	Gheath	Alat rash
Edgar	Gonzalez-Kozlova	Hsin-Hui	Huang
Mary W.	Redman	Hui	Xie
Hong	Chen	Manishkumar	Patel
Ganiraju C.	Manyam	Kai	Nie
Gayatri	Kumar	Jocelyn	Harris
Jianhua	Zhang	Kimberly	Argueta
Xingzhi	Song	James	Lindsay
Rossana	Lazcano	Roshni	Biswas
Mario L.	Marques-Piubelli	Stephen	Van Nostrand
Caddie	Laberiano-Fernandez	Seunghee	Kim-Schulze
Frank	Rojas	Jhanelle E.	Gray
Baili	Zhang	Roy	Herbst
Len	Taing	Ignacio I.	Wistuba
Aashna	Jhaveri	Scott	Gettinger
Jacob	Geisberg	Karen	Kelly
Jennifer	Altreuter	Lyudmila	Bazhenova
Franziska	Michor	Sacha	Gnjatic
James	Provencher	J. Jack	Lee
Joyce	Yu	Jianjun	Zhang
Ethan	Cerami	Cara	Haymaker
Radim	Moravec		